arXiv:1512.04159v1 [astro-ph.GA] 14 Dec 2015

CO($J = 3 - 2$) On-the-fly Mapping of the Nearby Spiral Galaxies NGC 628 and NGC 7793: Spatially-resolved CO($J = 3 - 2$) Star-formation Law

Kazuyuki MURAOKA[1], Miho TAKEDA[1], Kazuki YANAGITANI[1], Hiroyuki KANEKO[2], Kouichiro NAKANISHI[3,4], Nario KUNO[5], Kazuo SORAI[6], Tomoka TOSAKI[7], and Kotaro KOHNO[8]

[1]Department of Physical Science, Osaka Prefecture University, Gakuen 1-1, Sakai, Osaka 599-8531

[2]Nobeyama Radio Observatory, Minamimaki, Minamisaku, Nagano 384-1305

[3]National Astronomical Observatory of Japan, 2-21-1 Osawa, Mitaka, Tokyo 181-8588

[4]SOKENDAI (The Graduate University for Advanced Studies), 2-21-1 Osawa, Mitaka, Tokyo 181-0015

[5]Graduate School of Pure and Applied Sciences, University of Tsukuba, 1-1-1 Tennodai, Tsukuba, Ibaraki 305-8577

[6]Division of Physics, Graduate School of Science, Hokkaido University, Sapporo 060-0810

[7]Department of Geoscience, Joetsu University of Education, Joetsu, Niigata 943-8512

[8]Institute of Astronomy, The University of Tokyo, 2-21-1 Osawa, Mitaka, Tokyo 181-0015

*E-mail: kmuraoka@p.s.osakafu-u.ac.jp

Received ; Accepted

Abstract

We present the results of CO($J = 3 - 2$) on-the-fly mappings of two nearby non-barred spiral galaxies NGC 628 and NGC 7793 with the Atacama Submillimeter Telescope Experiment at an effective angular resolution of 25″. We successfully obtained global distributions of CO($J = 3 - 2$) emission over the entire disks at a sub-kpc resolution for both galaxies. We

examined the spatially-resolved (sub-kpc) relationship between CO($J = 3 - 2$) luminosities ($L'_{\rm CO(3-2)}$) and infrared (IR) luminosities ($L_{\rm IR}$) for NGC 628, NGC 7793, and M 83, and compared it with global luminosities of JCMT Nearby Galaxy Legacy Survey sample. We found a striking linear $L'_{\rm CO(3-2)} - L_{\rm IR}$ correlation over the 4 orders of magnitude, and the correlation is consistent even with that for ultraluminous infrared galaxies and submillimeter selected galaxies. In addition, we examined the spatially-resolved relationship between CO($J = 3 - 2$) intensities ($I_{\rm CO(3-2)}$) and extinction-corrected star formation rates (SFRs) for NGC 628, NGC 7793, and M 83, and compared it with that for GMCs in M 33 and 14 nearby galaxy centers. We found a linear $I_{\rm CO(3-2)} - {\rm SFR}$ correlation with ~ 1 dex scatter. We conclude that the CO($J = 3 - 2$) star formation law (i.e., linear $L'_{\rm CO(3-2)} - L_{\rm IR}$ and $I_{\rm CO(3-2)} - {\rm SFR}$ correlations) is universally applicable to various types and spatial scales of galaxies; from spatially-resolved nearby galaxy disks to distant IR-luminous galaxies, within ~ 1 dex scatter.

Key words: galaxies: ISM —galaxies: individual (NGC 628, NGC 7793) —galaxies: star formation

1 Introduction

Star formation is one of the most fundamental processes in the evolutions of galaxies from nearby objects to high-redshift ones. The star-formation law, which is a quantitative relationship between star formation rates (SFRs) and surface mass densities of molecular gas, is represented as a simple power-law and it is often referred to as the Schmidt-Kennicutt law (e.g., Schmidt 1959; Kennicutt 1998a). Recently, variations in the power-law index and dispersion of the star-formation law according to the differences in star-formation environments and physical/chemical properties of molecular gas have been investigated by several authors on the basis of low-J CO observations. For example, Daddi et al. (2010) suggested two different star formation modes in the gas mass versus SFR plane. One is a rapid starburst mode appropriate for ultraluminous infrared galaxies (ULIRGs), submillimeter selected galaxies, and local starbursts, and the other is a long-lasting mode appropriate for normal galaxy disks. The former mode shows about 1 dex higher star formation efficiencies (SFEs, defined as SFR per unit gas mass) than the latter mode. Such bimodal behavior of the star-formation law may be due to the effects of a top-heavy initial mass function in starbursts and/or the difference in dense gas fraction (e.g., Miura et al. 2014 and references therein). Krumholz et al. (2012) provided a theoretical explanation for such a disk-starburst bimodality. The authors showed that their sample

from Galactic clouds to submillimeter galaxies all lie on a single star formation law in which the SFR is simply $\sim 1\%$ of the molecular gas mass per local free-fall time. Leroy et al. (2013) demonstrated a first-order linear correspondence between surface densities of molecular gas and SFRs but also found second-order systematic variations for 30 nearby galaxies at a spatial resolution of 1 kpc. The authors found that the apparent molecular gas depletion time, which is an inverse of SFE, decreases with the decrease in stellar mass, metallicity, and dust-to-gas ratio. This can be explained by a CO-to-H_2 conversion factor that depends on dust shielding.

In order to understand the relationship between molecular gas and SFR further, higher-J CO transition gives an important clue because it can directly trace star-forming denser molecular medium owing to its high critical density. For instance, the star-formation law based on CO($J = 3 - 2$) emission (its critical density for collisional excitation is $\sim 10^4$ cm^{-3}) is often reported. Single-pointing CO($J = 3 - 2$) emission observations toward central regions of nearby galaxies or entire disks of distant galaxies showed the nearly linear correlations between CO($J = 3 - 2$) line intensities and SFRs (or between CO($J = 3 - 2$) luminosities, $L'_{\rm CO(3-2)}$, and infrared (IR) luminosities, $L_{\rm IR}$) with a better correlation coefficient than those based on CO($J = 1 - 0$) emission (e.g., Narayanan et al. 2005; Komugi et al. 2007; Iono et al. 2009; Mao et al. 2010), which suggests that measurements of CO($J = 3 - 2$) intensities correspond to a simple count of star-forming dense cores within the observing beam (see also Greve et al. 2014 and Liu et al. 2015 for similar CO to $L_{\rm IR}$ relations in higher-J transitions).

Obtaining wide-area and spatially-resolved CO($J = 3 - 2$) maps of galaxies is also important to examine the relationship between dense molecular gas and star formation in galaxy disks. An extensive CO($J = 3 - 2$) imaging survey of nearby galaxies is conducted using James Clerk Maxwell Telescope (JCMT). For example, Wilson et al. (2009) performed the CO($J = 3 - 2$) mapping of some members of Virgo Clusters (NGC 4254, NGC 4321, and NGC 4569), and examined a spatial variations in the gas properties traced by CO($J = 3 - 2$)/CO($J = 1 - 0$) intensity ratio (hereafter $R_{3-2/1-0}$). The authors found that NGC 4254 has a remarkably uniform $R_{3-2/1-0}$ of 0.33, whereas NGC 4569 shows a significant gradient from north to south in $R_{3-2/1-0}$; from 0.53 at the northern CO($J = 3 - 2$) peak to just 0.06 at the southern peak. Warren et al. (2010) presented the CO($J = 3 - 2$) mapping of three nearby field galaxies (NGC 628, NGC 3521, and NGC 3627), and found that SFE of the dense molecular gas traced by CO($J = 3 - 2$) emission (i.e., $\propto$ SFR divided by $L'_{\rm CO(3-2)}$) mostly independent or only weakly dependent on molecular gas density, $R_{3-2/1-0}$, and the fraction of total gas in molecular form. Wilson et al. (2012) examined the correlation between global $L'_{\rm CO(3-2)}$ and far-IR (FIR) luminosities ($L_{\rm FIR}$) for more than 30 galaxies. The authors found a remarkably tight $L'_{\rm CO(3-2)} - L_{\rm FIR}$ correlation among IR-luminous galaxies (i.e., $L_{\rm FIR}/L'_{\rm CO(3-2)}$ ratios are constant

among IR-luminous galaxies), whereas $L_{\rm FIR}/L'_{\rm CO(3-2)}$ ratios (and their scatter) tend to increase among the fainter galaxies.

Another extra-galactic CO($J=3-2$) imaging survey of nearby spiral galaxies has been made using the Atacama Submillimeter Telescope Experiment (ASTE: Ezawa et al. 2004; Ezawa et al. 2008), and obtained sensitive CO($J=3-2$) images of M 83 (Muraoka et al. 2007; Muraoka et al. 2009), M 33 (Tosaki et al. 2007; Miura et al. 2012; Miura et al. 2014), and NGC 986 (Kohno et al. 2008). We found a linear correlation between CO($J=3-2$) intensities and extinction-corrected Hα luminosities over the whole disk of M 83 (Muraoka et al. 2009). However, in order to reveal the "universal" star-formation law in galaxies based on CO($J=3-2$) emission further, it is indispensable to examine its dependence on various galaxy properties and environments, such as density and temperature of molecular gas, metallicity, and the difference between nuclear starbursts and star-forming regions in galaxy disks with an adequate spatial resolution (≤ 1 kpc). We therefore need to increase the number of spatially-resolved studies of the CO($J=3-2$) star-formation law covering whole disks of nearby galaxies with various galaxy properties and environments.

In this paper, we present wide-area CO($J=3-2$) images of nearby non-barred spiral galaxies NGC 628 and NGC 7793 using the ASTE, employing an on-the-fly (OTF) mapping mode. Basic parameters of each galaxy are summarized in table 1. The distances to NGC 628 and NGC 7793 are estimated to be 7.3 Mpc and 3.91 Mpc (Karachentsev et al. 2004); therefore, the effective beam size of ASTE, $25''$, corresponds to 900 pc and 480 pc, respectively. This enables us to resolve major structures (i.e., the center and spiral arms) at a sub-kpc resolution. NGC 628 and NGC 7793 are suitable targets to examine a spatially-resolved CO($J=3-2$) star-formation law and to compare it with that in M 83 because the distance to M 83 is estimated to 4.5 Mpc (Thim et al. 2003), which is similar to NGC 628 and NGC 7793. And more importantly, the star-formation environment in M 83 is different from these two galaxies; M 83 hosts a nuclear starburst, while NGC 628 and NGC 7793 are normal disk galaxies without strong nuclear activities. Thus, we can investigate the difference in the CO($J=3-2$) star-formation law between the starbursts and star-forming regions in galaxy disks. These galaxies are rich in multi-wavelength data set to calculate SFRs, such as Hα and IR images, since these galaxies are the targets of the $Spitzer$ Infrared Nearby Galaxies Survey (SINGS: Kennicutt et al. 2003) and/or the Local Volume Legacy (LVL) survey project (Kennicutt et al. 2008; Dale et al. 2009).

The goals of this paper are: (1) to reveal the global distributions of CO($J=3-2$) emission in NGC 628 and NGC 7793, (2) to measure CO($J=3-2$) intensities ($I_{\rm CO(3-2)}$) and $L'_{\rm CO(3-2)}$, and examine $R_{3-2/1-0}$ in these two galaxies, (3) to examine the spatially-resolved (sub-kpc) CO($J=3-2$) star-formation law (i.e., $L'_{\rm CO(3-2)}-L_{\rm IR}$ and $I_{\rm CO(3-2)}-{\rm SFR}$ correlations) for NGC 628, NGC 7793, and M 83, and to compare the obtained CO($J=3-2$) star-formation law with earlier studies, and (4)

to investigate the dependence of the CO($J=3-2$) star-formation law on star-formation environments (i.e., the difference among ULIRGs, submillimeter selected galaxies, local starbursts, and normal star-forming regions in galaxy disks).

2 Observations and Data Reduction

CO($J=3-2$) emission observations of NGC 628 and NGC 7793 were performed using the ASTE 10-m dish from September to October, 2013, and July to August, 2014, respectively. The sizes of CO($J=3-2$) maps are $6' \times 6'$ (12.8 kpc $\times$ 12.8 kpc) for NGC 628 and $5' \times 5'$ (5.8 kpc $\times$ 5.8 kpc) for NGC 7793. The mapped area in each galaxy is indicated in figure 1.

We used a waveguide-type sideband-separating SIS mixer receiver for the single side band (SSB) operation, CATS345 (Ezawa et al. 2008; Inoue et al. 2008). The typical image rejection ratio of CATS345 was estimated to be ~ 10 dB at the frequency in which CO($J=3-2$) emission was observed. The backend we used was a digital autocorrelator system, MAC (Sorai et al. 2000), which comprises four banks of a 512 MHz wide spectrometer with 1024 spectral channels each. This arrangement provided a velocity coverage of 440 km s^{-1} with a velocity resolution of 0.43 km s^{-1}. Since the observations were carried out in excellent atmospheric conditions (the zenith opacity of 220 GHz ranged from 0.03 to 0.10), the system noise temperature was typically $200-300$ K (in SSB). We performed the OTF mapping along two different directions (i.e., scans along the R.A. and Decl. directions), and these two data sets were co-added by the Basket-weave method (Emerson & Graeve 1988).

We periodically observed CO($J=3-2$) emission of M 17 SW and CW Leo to obtain the main beam efficiency $\eta_{\rm MB}$ in each observing run. We compared our CO($J=3-2$) spectra with those obtained by CSO observations (Wang et al. 1994), and $\eta_{\rm MB}$ was estimated to be $0.54-0.60$ for observing runs in 2013 (NGC 628) and $0.60-0.70$ for those in 2014 (NGC 7793). The absolute error of the CO($J=3-2$) temperature scale was about $\pm$ 20%, mainly due to variations in $\eta_{\rm MB}$ and the image rejection ratio of the CATS345. Observation parameters are summarized in table 2.

The data reduction was conducted using the software package NOSTAR, which comprises tools for OTF data analysis, developed by NAOJ (Sawada et al. 2008). The raw data were regridded to $7''.5$ per pixel, giving an effective angular resolution of $\sim 25''$. Linear baselines were subtracted from the spectra. In addition, we subtracted third-order baseline from a portion of the spectra whose line width are sufficiently narrow ($<$ 40 km s^{-1}), which do not influence line profiles of CO($J=3-2$) emission. We binned the adjacent channels to a velocity resolution of 5 km s^{-1} for the CO($J=3-2$) spectra. Finally, 3D data cubes were created. The resultant r.m.s. noise level (1 σ) in $T_{\rm MB}$ scale at

a beam size of 25″ (HPBW) was typically ~ 25 mK and ~ 11 mK for NGC 628 and NGC 7793, respectively.

3 Results

3.1 CO($J = 3-2$) Channel Maps, Intensities, and Luminosities

The derived velocity channel maps of CO($J = 3-2$) emission in NGC 628 and NGC 7793 are shown in figure 2 and figure 3, respectively. No strong concentration of CO($J = 3-2$) emission toward central regions are found in either galaxy, which is different from previous our CO($J = 3-2$) sample, barred spiral galaxies M 83 and NGC 986, showing strong peaks at their centers.

We calculated the velocity-integrated intensities of CO($J = 3-2$) emission (i.e., $I_{\rm CO(3-2)}$) in NGC 628 and NGC 7793 with a noise cut-off level of 2σ and created their maps as shown in figure 4. We successfully obtained the global CO($J = 3-2$) distributions at a sub-kpc resolution for both galaxy disks; we note that this is the first global CO image of NGC 7793 at all the transitions. The CO($J = 3-2$) image of NGC 628 is similar to that obtained with the JCMT (Warren et al. 2010; Wilson et al. 2012), yet our map depicts even CO($J = 3-2$) emission extending southward along the spiral arm. We compare the distributions of CO($J = 3-2$) emission with $Herschel$/SPIRE 350 μm emission obtained by the KINGFISH (Key Insights on Nearby Galaxies: a Far-Infrared Survey with $Herschel$) project (Kennicutt et al. 2011). In figure 5, we find a good spatial coincidence between CO($J = 3-2$) emission and 350 μm emission for each galaxy, which suggests the coexistence of the dense molecular medium and the cold dust component.

We summarize the peak intensity of CO($J = 3-2$) emission and its location in each galaxy. For NGC 628, we found the peak intensity in our CO($J = 3-2$) map of 2.7 $\pm$ 0.5 K km s^{-1} in $T_{\rm MB}$ scale at 25″ resolution. This peak value occurs at several positions across the map, including the nucleus as well as several local peaks along spiral arms. According to Warren et al. (2010), the strongest $I_{\rm CO(3-2)}$ observed with the JCMT is 3.7 $\pm$ 0.5 K km s^{-1} at 15″ resolution. These two values of $I_{\rm CO(3-2)}$ seem in good agreement if we consider the difference in the angular resolution and the extended distribution of CO($J = 3-2$) emission. For NGC 7793, we found the peak intensity in our CO($J = 3-2$) map of 1.5 $\pm$ 0.3 K km s^{-1} in $T_{\rm MB}$ scale at 25″ resolution, which is observed not at the center but in the disk. The central $I_{\rm CO(3-2)}$ is only 0.7 $\pm$ 0.1 K km s^{-1}.

We have calculated the global and central $L'_{\rm CO(3-2)}$, and compared them with those reported in earlier studies. The $L'_{\rm CO(3-2)}$ is calculated as follows:

$$L'_{\rm CO(3-2)} = I_{\rm CO(3-2)}\, D^2\, \Omega \quad {\rm K\ km\ s^{-1}\ pc^2}, \tag{1}$$

where D is the distance of a galaxy in pc, and Ω is the covered area in rad^2. For NGC 628, we found

the global $L'_{\rm CO(3-2)}$ = (7.1 $\pm$ 1.6) $\times$ 10^7 K km s^{-1} pc^2 over the observed $6' \times 6'$ region. This value is slightly higher than that obtained by Wilson et al. (2012), 5.2 $\times$ 10^7 K km s^{-1} pc^2. However, their $L'_{\rm CO(3-2)}$ was calculated for a smaller area, $5' \times 5'$. We recalculated our global $L'_{\rm CO(3-2)}$ over the same $5' \times 5'$ region, and found $L'_{\rm CO(3-2)}$ = (6.4 $\pm$ 1.4) $\times$ 10^7 K km s^{-1} pc^2, which is in agreement with that obtained by Wilson et al. (2012). In addition, we obtained $L'_{\rm CO(3-2)}$ within the central 1 kpc in NGC 628 of (4.3 $\pm$ 0.9) $\times$ 10^6 K km s^{-1} pc^2, and found the ratio of the central $L'_{\rm CO(3-2)}$ to the global $L'_{\rm CO(3-2)}$ is only 0.061. This is significantly smaller than that obtained in M 83, 0.22 (Muraoka et al. 2007).

For NGC 7793, we found the global $L'_{\rm CO(3-2)}$ = (7.4 $\pm$ 1.4) $\times$ 10^6 K km s^{-1} pc^2 over the observed $5' \times 5'$ region, which is an order of magnitude lower than that in NGC 628. This is partly because the total H_2 mass in NGC 7793, $2.0 \times 10^8 M_\odot$ (calculated from the CO($J = 1 - 0$) intensity obtained by Israel et al. 1995), is also an order of magnitude lower than that in NGC 628, $1.51 \times 10^9 M_\odot$ (Garnett 2002). In addition, we obtained $L'_{\rm CO(3-2)}$ = (4.2 $\pm$ 0.8) $\times$ 10^5 K km s^{-1} pc^2 within the central 1 kpc of NGC 7793, and found the ratio of the central $L'_{\rm CO(3-2)}$ to the global $L'_{\rm CO(3-2)}$ of 0.055, which is comparable to that in NGC 628. Therefore, the contribution of the central $L'_{\rm CO(3-2)}$ to the global $L'_{\rm CO(3-2)}$ is less than 10 % for these two spiral galaxies without strong nuclear activity.

We examined the correlation between global $L'_{\rm CO(3-2)}$ and $L_{\rm FIR}$ for NGC 628, NGC 7793, M 83 (Muraoka et al. 2009), and galaxies in JCMT Nearby Galaxy Legacy Survey (NGLS) sample (Wilson et al. 2012). We calculated $L_{\rm FIR}$ of ASTE sample (NGC 628, NGC 7793, and M 83) from the original data presented by Sanders et al. (2003) for adopted distance. Figure 6 shows the correlation between $L'_{\rm CO(3-2)}$ and $L_{\rm FIR}$ and the variation in $L_{\rm FIR}/L'_{\rm CO(3-2)}$ as a function of $L'_{\rm CO(3-2)}$. Our ASTE sample reinforces the tight correlation between $L'_{\rm CO(3-2)}$ and $L_{\rm FIR}$, and the declining tendency of $L_{\rm FIR}/L'_{\rm CO(3-2)}$ with the increase in $L'_{\rm CO(3-2)}$ demonstrated by Wilson et al. (2012).

3.2 CO($J = 3 - 2$)/CO($J = 1 - 0$) Intensity Ratios $R_{3-2/1-0}$

Here, we examine $R_{3-2/1-0}$ in NGC 628 and NGC 7793 to estimate the average physical condition of molecular gas within the observing beam.

We used the CO($J = 1 - 0$) image in NGC 628 obtained with the Berkeley-Illinois-Maryland Association millimeter interferometer Survey of Nearby Galaxies (BIMA SONG: Helfer et al. 2003) project, which is convolved to an angular resolution of 25″ to match our CO($J = 3 - 2$) image. We can obtain $R_{3-2/1-0}$ only in the central $\sim 3' \times 3'$ region due to the smaller coverage of the BIMA CO($J = 1 - 0$) image. According to the pixel-by-pixel comparison of each CO map, the obtained $R_{3-2/1-0}$ are in the range of 0.1 to 1.1. We found that $\sim$70% of pixels show lower $R_{3-2/1-0}$, $0.10 - 0.60$, regardless

of galactocentric distance, and found that the global $R_{3-2/1-0}$ over the $\sim 3' \times 3'$ region is estimated to be 0.39, which are well consistent with those reported by Warren et al. (2010) and Wilson et al. (2012). Note that pixels with higher $R_{3-2/1-0}$ ($\geq$ 1.0) are not adjacent each other, i.e., exist locally. A similar situation has been observed in M 83; the average $R_{3-2/1-0}$ in the disk ($r > 1$ kpc) of M 83 is $0.6 - 0.7$, but there exists some locations where $R_{3-2/1-0}$ exceed 1.2 (Muraoka et al. 2007). Such local peaks of $R_{3-2/1-0}$ are presumably due to the uncertainties and the poor signal-to-noise ratio of both CO data.

We compare the obtained $R_{3-2/1-0}$ in NGC 628 with those in various types of galaxies. Firstly, we summarize $R_{3-2/1-0}$ in normal spiral galaxies. The mean $R_{3-2/1-0}$ are $0.4 - 0.5$ for giant molecular clouds (GMCs) in the disk of the Milky Way (Sanders et al. 1993; Oka et al. 2007), $0.3 - 0.4$ for NGC 4254 and NGC 4321 (Wilson et al. 2009), and ~ 0.4 for the spiral arm of M 51 (Vlahakis et al. 2013). These values are almost comparable to the global $R_{3-2/1-0}$ of 0.39 in NGC 628. In addition, the distribution of spatially-resolved $R_{3-2/1-0}$ in M 51 ($0.1 - 0.7$: Vlahakis et al. 2013) is quite similar to that in NGC 628 (typically $0.10 - 0.60$). However, higher $R_{3-2/1-0}$ have been frequently observed in starburst galaxies. For example, the central $R_{3-2/1-0}$ in NGC 253 and M 82 are 0.8 and 1.0, respectively (Dumke et al. 2001). Moreover, Muraoka et al. (2007) reported that M 83 shows higher $R_{3-2/1-0}$ both in the central region (~ 1.0) and in the disk ($0.6 - 0.7$). This suggests that dense gas fraction traced by $R_{3-2/1-0}$ in starburst galaxies is higher than that in NGC 628. Lastly, we compare $R_{3-2/1-0}$ in NGC 628 and those in early-type galaxies. According to Mao et al. (2010), single-pointing $R_{3-2/1-0}$ in early-type galaxies are typically in the range of $0.3 - 0.5$, which are comparable to that in NGC 628, while some early-type galaxies (NGC 7077 and NGC 7679) show higher $R_{3-2/1-0}$ (> 1.0). The reason of such a great difference in $R_{3-2/1-0}$ among early-type galaxies is unclear, but this is presumably due to the difference in the physical condition of molecular gas in each galaxy.

For NGC 7793, there is no available CO($J = 1 - 0$) map, but Israel et al. (1995) obtained CO($J = 1 - 0$) spectrum in the central region using the SEST 15-m telescope at an angular resolution of $43''$. In order to obtain the central $R_{3-2/1-0}$, we convolved our CO($J = 3 - 2$) data ($25''$) to the same angular resolution ($43''$). The convolved CO($J = 3 - 2$) spectrum in the central region is shown in figure 7. The significant emission can be seen in the velocity range of 200 to 300 km s^{-1}, which is consistent with the central H I emission obtained with the NRAO Very Large Array (Walter et al. 2008). Within this velocity range, we obtained the central $I_{\rm CO(3-2)}$ at an angular resolution of $43''$ of 0.46 $\pm$ 0.07 K km s^{-1} in $T_{\rm MB}$ scale. We calculated the central CO($J = 1 - 0$) intensity ($I_{\rm CO(1-0)}$) in the same velocity range as our CO($J = 3 - 2$) emission based on the CO($J = 1 - 0$) spectrum shown in figure 2 of Israel et al. (1995). We obtained $I_{\rm CO(1-0)}$ of 2.7 $\pm$ 0.4 K km s^{-1}, which gives $R_{3-2/1-0}$

of 0.17 $\pm$ 0.06.

The central $R_{3-2/1-0}$ in NGC 7793, 0.17 $\pm$ 0.06, is considerably lower than those reported by earlier studies based on single-pointing observations of external galaxies. For example, Mauersberger et al. (1999) found that $R_{3-2/1-0}$ in 28 nearby galaxies are in the range of 0.2 to 0.7, and Mao et al. (2010) reported that $R_{3-2/1-0}$ are in the range of 0.2 to 1.9 for their sample including various types of galaxies; normal, Seyfert, starburst galaxies, and luminous infrared galaxies (LIRGs). In addition, Meier et al. (2001) found that $R_{3-2/1-0}$ in dwarf starburst galaxies are in the range of 0.34 to 2.6, and $R_{3-2/1-0}$ in compact galaxies are in the range of 0.63 to 1.5 (Israel 2005). However, such a low $R_{3-2/1-0}$ (< 0.20) is sometimes observed as the local minimum in galaxy disks. In fact, we found the smallest $R_{3-2/1-0}$ of 0.10 in the inter-arm of NGC 628 as described above. In addition, Onodera et al. (2012) found GMCs with $R_{3-2/1-0} \sim 0.1-0.2$ in the second nearest spiral galaxy M 33. These GMCs with low $R_{3-2/1-0}$ are widely distributed over the disk in M 33, and their masses are small (typically less than $10^5 M_\odot$). This suggests that such less massive GMCs ($< 10^5 M_\odot$) are dominant in the central region of NGC 7793 if we assume the filling factor of CO($J = 3-2$) emission is comparable to that of CO($J = 1-0$) emission.

Some theoretical models are utilized to obtain the physical interpretation of observed $R_{3-2/1-0}$. In particular, the Large Velocity Gradient (LVG) approximation (Scoville & Solomon 1974; Goldreich & Kwan 1974) and the photo-dissociation region (PDR) models (e.g., Hollenbach & Tielens 1997; Hollenbach & Tielens 1999; Kaufman et al. 1999) are widely applied to derive physical parameters, such as density ($n_{\rm H_2}$) and kinetic temperature ($T_{\rm K}$) of molecular gas. For example, if we assume a CO fractional abundance per unit velocity gradient $Z(^{12}{\rm CO})/(dv/dr)$ of 1×10^{-4} and a moderate $T_{\rm K}$ of 30 K under the LVG approximation with a one-zone assumption, the observed $R_{3-2/1-0}$ of 0.39 in NGC 628 and 0.17 in NGC 7793 correspond to low $n_{\rm H_2}$ of $\sim 10^{2.5}$ cm^{-3} and $\sim 10^{2.1}$ cm^{-3}, respectively. However, a different physical condition can reproduce the same $R_{3-2/1-0}$ value under the LVG approximation; a moderate $n_{\rm H_2}$ of $10^{3.2}$ cm^{-3} and a low $T_{\rm K}$ of 10 K also yield the $R_{3-2/1-0}$ of 0.17. Therefore, it is difficult to decide whether a low $R_{3-2/1-0}$ of 0.17 observed in NGC 7793 is attributable to the decrease in $n_{\rm H_2}$ or that in $T_{\rm K}$.

4 Discussion

Validity of a use of CO($J = 3-2$) emission as a dense gas tracer, and its correlation with SFRs and (F)IR luminosities have been energetically studied by many authors. For example, inclination-corrected $I_{\rm CO(3-2)}$ were compared with extinction-corrected SFRs for 14 nearby galaxy centers by Komugi et al. (2007). The authors found the strong correlation between these 2 quantities with a

linear slope of 1.0.

The detailed investigation of the $L'_{\rm CO(3-2)} - L_{\rm FIR}$ correlation is first performed by Yao et al. (2003). They found a superlinear slope of 1.4 for 60 IR luminous galaxies. However, recent studies reported that the reanalysis of Yao et al. (2003) data yields a linear slope of 1.0 (Mao et al. 2010; Greve et al. 2014). In addition, Narayanan et al. (2005) found the nearly linear correlation between $L'_{\rm CO(3-2)}$ and $L_{\rm IR}$ for 17 starburst spiral galaxies, LIRGs, and ULIRGs. The obtained $L'_{\rm CO(3-2)} - L_{\rm IR}$ slope is 0.92. Subsequent studies also report nearly linear $L'_{\rm CO(3-2)} - L_{\rm FIR}$ (and/or $L'_{\rm CO(3-2)} - L_{\rm IR}$) correlations. The reported slopes are 1.08 for LIRGs, submillimeter selected galaxies, quasars, and Lyman-break galaxies (Iono et al. 2009), 0.99 for nearby ($D < 10$ Mpc) and high-z ($z \geq 1$) sources (Bayet et al. 2009), 0.87 for 114 targets including normal, Seyfert, starburst galaxies, and luminous infrared galaxies (Mao et al. 2010), and $0.99 - 1.00$ for a sample of 62 local (U)LIRGs and 35 submillimeter selected dusty star-forming galaxies (Greve et al. 2014).

Here, we investigate whether such a linear correlation based on CO($J = 3-2$) emission is commonly applicable to each local position in nearby spiral galaxies. Firstly, we examine the spatially-resolved (sub-kpc) $L'_{\rm CO(3-2)} - L_{\rm IR}$ ($8 - 1000$ μm) correlation for NGC 628, NGC 7793, and M 83. We use the CO($J = 3-2$) image of M 83 obtained by Muraoka et al. (2009). In addition, we compare the obtained $L'_{\rm CO(3-2)} - L_{\rm IR}$ correlation with global luminosities for JCMT NGLS sample (Wilson et al. 2012) and the best-fit relation, log $L_{\rm IR}$ = (1.00 $\pm$ 0.05) log $L'_{\rm CO(3-2)}$ + (2.2 $\pm$ 0.5), for the local (U)LIRGs and submillimeter selected dusty star-forming galaxies (Greve et al. 2014). We obtain $L_{\rm IR}$ for JCMT NGLS sample from Sanders et al. (2003) for adopted distances. Second, we examine the spatially-resolved relationship between $I_{\rm CO(3-2)}$ and SFRs based on extinction-corrected Hα luminosities for NGC 628, NGC 7793, and M 83. We compare the obtained $I_{\rm CO(3-2)} - {\rm SFR}$ correlation with that for GMCs in M 33 and 14 nearby galaxy centers. We use the single-pointing $I_{\rm CO(3-2)}$ and SFRs of GMCs in M 33 at the spatial resolution of ~ 100 pc obtained by Onodera et al. (2012) and those of 14 nearby galaxy centers summarized by Komugi et al. (2007).

4.1 Correlation between Spatially-resolved $L'_{\rm CO(3-2)}$ and $L_{\rm IR}$

Generally, $L_{\rm IR}$ are calculated from flux densities of multiple IR-bands, but this makes the estimate of spatially-resolved $L_{\rm IR}$ in nearby galaxy disks difficult. Dale et al. (2009) examined the monochromatic-to-bolometric infrared ratios for globally integrated LVL data. The authors reported that the $Spitzer$/MIPS 70 μm and 160 μm emission are tightly coupled to the bolometric IR emission. Indeed, the mean 70 μm-to-total IR (TIR; $3 - 1100$ μm) luminosity ratio is 0.46 with a smaller scatter of 0.11 dex. Thus, we use MIPS 70 μm images obtained by the LVL survey to estimate the

spatially-resolved $L_{\rm IR}$ for NGC 628, NGC 7793, and M 83.

First, we examined the global 70 μm luminosity (L_{70}) to $L_{\rm IR}$ ratio ($L_{70}/L_{\rm IR}$) for each galaxy. The global 70 μm luminosities are calculated from the integrated MIPS 70 μm flux densities summarized by Dale et al. (2009), and the $L_{\rm IR}$ are obtained from Sanders et al. (2003). The resultant global $L_{70}/L_{\rm IR}$ are 0.51, 0.61, and 0.53 for NGC 628, NGC 7793, and M 83, respectively. These values are slightly greater than the mean ratio of 0.46 reported by Dale et al. (2009). This is because the wavelength range of their TIR luminosity ($L_{\rm TIR}$; $3-1100$ μm) is wider than that of $L_{\rm IR}$ ($8-1000$ μm), and thus $L_{\rm TIR}$ is definitely greater than $L_{\rm IR}$ (i.e., $L_{70}/L_{\rm IR}$ is greater than $L_{70}/L_{\rm TIR}$). Then, we converted the spatially-resolved L_{70} to $L_{\rm IR}$ for each pixel by using the global $L_{70}/L_{\rm IR}$ of each galaxy as a "scaling" factor. Note that we cannot consider the local variations in $L_{70}/L_{\rm IR}$ within each galaxy disk, and thus we estimated the absolute error of $L_{\rm IR}$ in each pixel of ±30% considering the scatter of $L_{70}/L_{\rm TIR}$ of 0.11 dex (~ 30%) (Dale et al. 2009).

For the pixel-by-pixel comparison between $L'_{\rm CO(3-2)}$ and $L_{\rm IR}$, we used pixels whose $L'_{\rm CO(3-2)}$ exceed 3 σ corresponding to 5.6×10^5 K km s^{-1} pc^2, 8.5×10^4 K km s^{-1} pc^2, and 7.0×10^5 K km s^{-1} pc^2 for NGC 628, NGC 7793, and M 83, respectively. In this analysis, we divided M 83 data into two regions according to the galactocentric radius; the central region ($r\leq1$ kpc) and the disk ($r>1$ kpc), in order to distinguish the nuclear starburst and star-forming regions in the disk.

Figure 8 shows the obtained $L'_{\rm CO(3-2)}-L_{\rm IR}$ correlation. We found a striking linear correlation over the 4 orders of magnitude. $L_{\rm IR}$ at a given $L'_{\rm CO(3-2)}$ seems typically smaller than the best-fit relation for the sample of Greve et al. (2014) by $0.3-0.5$ dex, but is almost within the error of the best-fit relation. Note that we found only weak $L'_{\rm CO(3-2)}-L_{\rm IR}$ correlations for NGC 628 and NGC 7793 individually, with Spearman rank correlation coefficients of 0.31 and 0.23, respectively. This is presumably due to the lack of the dynamic range in $L'_{\rm CO(3-2)}$, only ~0.5 dex for NGC 628 and NGC 7793, which is comparable to the scatter in $L_{\rm IR}$ at a given $L'_{\rm CO(3-2)}$; therefore, an individual $L'_{\rm CO(3-2)}-L_{\rm IR}$ correlation for each galaxy becomes weaker. In order to obtain a strong $L'_{\rm CO(3-2)}-L_{\rm IR}$ correlation for an individual galaxy, it is necessary to ensure an enough dynamic range in $L'_{\rm CO(3-2)}$ at least an order of magnitude such as M 83. The important thing is that almost all data points lie on a single $L'_{\rm CO(3-2)}-L_{\rm IR}$ correlation in figure 8.

In figure 8, we also found a bimodal correlation for each subsample; we obtained the best-fit slope for the spatially-resolved sample (NGC 628, NGC 7793, and M 83) of 0.84, and that for the JCMT NGLS sample of 0.74, in spite of the linear $L'_{\rm CO(3-2)}-L_{\rm IR}$ correlation for the combined sample. This is because the luminosities (both $L'_{\rm CO(3-2)}$ and $L_{\rm IR}$) are proportional to the coverer area (i.e., $D^2\Omega$ in equation 1) in a linear scale (pc^2). In fact, $D^2\Omega$ at sub-kpc resolution of $\sim10^5$ pc^2 is 2 or 3 orders of magnitude smaller than that for a global galaxy disk of 10^7-10^8 pc^2. Such a difference

in $D^2\Omega$ among each sample automatically produces the linear $L'_{\rm CO(3-2)} - L_{\rm IR}$ correlation for the combined sample over the 3 orders of magnitude even if the slope of $L'_{\rm CO(3-2)} - L_{\rm IR}$ correlation for each subsample is sublinear.

The sublinear $L'_{\rm CO(3-2)} - L_{\rm IR}$ slope of 0.74 for the JCMT NGLS sample is consistent with the declining tendency of $L_{\rm FIR}/L'_{\rm CO(3-2)}$ ratio with the increase in $L'_{\rm CO(3-2)}$ reported by Wilson et al. (2012) (see also figure 6). The authors argued that fainter galaxies have lower average CO surface brightnesses, in which case they could systematically underestimate the CO luminosity due to the low signal-to-noise ratio.

The $L'_{\rm CO(3-2)} - L_{\rm IR}$ slope of 0.84 for our spatially-resolved sample seems slightly smaller than that reported by earlier studies (~ 1.0). However, we cannot discuss its significance yet because the slope of 0.84 is determined for only 3 galaxy sample in this study. Further analyses of the spatially-resolved $L'_{\rm CO(3-2)} - L_{\rm IR}$ correlation for more sample are required to determine more reliable $L'_{\rm CO(3-2)} - L_{\rm IR}$ slope and to understand its physical meaning in nearby galaxies.

4.2 Correlation between Spatially-resolved $I_{\rm CO(3-2)}$ and SFRs

Extinction-corrected SFRs are calculated from a linear combination of Hα and $Spitzer$/MIPS 24 μm luminosities as follows (Kennicutt 1998a; Kennicutt 1998b; Calzetti et al. 2007):

$$\mathrm{SFR} = 7.9 \times 10^{-42} \left(\frac{L_{\rm H\alpha} + 0.031 \times L_{24\mu\rm m}}{\rm erg\ s^{-1}} \right) \frac{\cos i}{\Omega_A} \quad M_\odot\ \mathrm{yr}^{-1}\ \mathrm{pc}^{-2}, \tag{2}$$

where $L_{\rm H\alpha}$ and $L_{24\mu\rm m}$ mean Hα and 24 μm luminosities, respectively. i is the inclination of each galaxy and Ω_A is the covered area within the 25″ beam (in the unit of pc^2). We used Hα and 24 μm images of NGC 7793 obtained by the SINGS and those of M 83 and NGC 628 by the LVL survey.

Figure 9 shows the obtained $I_{\rm CO(3-2)} - \mathrm{SFR}$ correlation. We found a linear correlation between $I_{\rm CO(3-2)}$ and extinction-corrected SFRs with ~ 1 dex scatter, whereas we also found a larger scatter (~ 2 orders of magnitude) for GMCs in M 33. This is presumably due to the small spatial resolution for M 33. Miura et al. (2012) reported that GMCs in M 33 are classified into four types according to their evolutional stages; i.e., the age of the associated young stellar groups and H II regions. This causes the difference in the estimated SFRs by $2-3$ orders of magnitude for every GMCs. In addition, the peak positions of CO($J=3-2$) emission for some GMCs are ~ 100 pc away from their associated H II regions. This spatial offset just corresponds to the observing beam of CO($J=3-2$) emission. For these reasons, the larger scatter for GMCs in M 33 in figure 9 is observed. Nonetheless, the overall $I_{\rm CO(3-2)} - \mathrm{SFR}$ correlation is still robust even if GMCs in M 33 are included.

Finally, we note the dependence of the obtained CO($J=3-2$) star-formation law on star-formation environments. As shown in figure 8 and figure 9, the $L'_{\rm CO(3-2)} - L_{\rm IR}$ and the $I_{\rm CO(3-2)} - \mathrm{SFR}$

correlations for the central region of M 83 is well consistent with those for NGC 628, NGC 7793, and the disk of M 83, and is consistent even with those for other sample in earlier studies (i.e., ULIRGs, submillimeter selected galaxies, whole disks of JCMT NGLS sample, 14 nearby galaxy centers, and GMCs in M 33). We conclude that the CO($J = 3 - 2$) star formation law (linear $L'_{\rm CO(3-2)} - L_{\rm IR}$ and $I_{\rm CO(3-2)} - {\rm SFR}$ correlations) is universally applicable to various types and spatial scales of galaxies; from spatially-resolved nearby galaxy disks to distant IR-luminous galaxies, within ~ 1 dex scatter.

5 Summary

We have performed CO($J = 3 - 2$) emission observations of the $6' \times 6'$ (or 12.8 $\times$ 12.8 kpc at the distance of 7.3 Mpc) region of the nearby spiral galaxy NGC 628 (M 74) and the $5' \times 5'$ (or 5.8 $\times$ 5.8 kpc at the distance of 3.91 Mpc) region of the nearby spiral galaxy NGC 7793 with the ASTE at an effective angular resolution of 25″. A summary of this work is as follows.

1. We successfully obtained global distributions of CO($J = 3 - 2$) emission over the entire disks at a sub-kpc resolution for both galaxies. In addition, we found that the CO($J = 3 - 2$) emission is well spatially coincident with the $Herschel$/SPIRE 350 μm emission.
2. We found that the global $L'_{\rm CO(3-2)}$ are (7.1 $\pm$ 1.6) $\times$ 10^7 K km s^{-1} pc^2 for NGC 628 and (7.4 $\pm$ 1.4) $\times$ 10^6 K km s^{-1} pc^2 for NGC 7793, respectively. We found that no central concentration of CO($J = 3 - 2$) emission; the ratios of the central (< 1 kpc) $L'_{\rm CO(3-2)}$ to the global $L'_{\rm CO(3-2)}$ are only ~ 0.06 for both galaxies.
3. We found the average $R_{3-2/1-0}$ in NGC 628 of 0.39, which may be a typical value in galaxy disks according to the comparison with earlier studies for galactic and extragalactic objects. On the other hand, we found the central $R_{3-2/1-0}$ at 43″ resolution in NGC 7793 of 0.17. Such a low $R_{3-2/1-0}$ was observed for less massive ($< 10^5 M_\odot$) GMCs in the disk of M 33, which suggests that such less massive GMCs are dominant in the central region of NGC 7793.
4. We examined the spatially-resolved (sub-kpc) $L'_{\rm CO(3-2)} - L_{\rm IR}$ correlation for NGC 628, NGC 7793, and M 83, and compared it with global luminosities of JCMT NGLS sample. We found a striking linear $L'_{\rm CO(3-2)} - L_{\rm IR}$ correlation over the 4 orders of magnitude, and the correlation is consistent even with that for (U)LIRGs and submillimeter selected galaxies.
5. We examined the spatially-resolved relationship between $I_{\rm CO(3-2)}$ and extinction-corrected SFRs for NGC 628, NGC 7793, and M 83, and compared it with that for GMCs in M 33 and 14 nearby galaxy centers. We found a linear $I_{\rm CO(3-2)} - {\rm SFR}$ correlation with ~ 1 dex scatter.
6. We conclude that the CO($J = 3 - 2$) star formation law (i.e., linear $L'_{\rm CO(3-2)} - L_{\rm IR}$ and $I_{\rm CO(3-2)} - {\rm SFR}$ correlations) is universally applicable to various types and spatial scales of galaxies; from

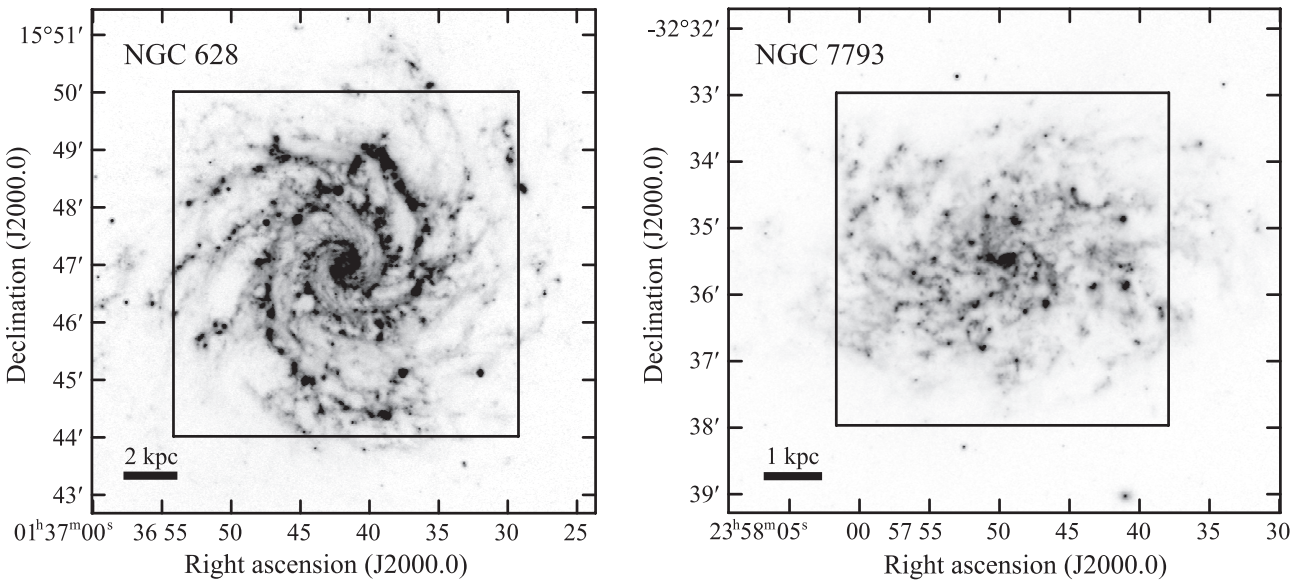


Fig. 1. Observed $6' \times 6'$ area of NGC 628 (left) and $5' \times 5'$ area of NGC 7793 (right), which are indicated by large squares, superposed on $Spitzer$/IRAC 8 μm images (Dale et al. 2009) in order to display footprints of the ASTE observations.

spatially-resolved nearby galaxy disks to distant IR-luminous galaxies, within ~ 1 dex scatter.

We thank the referee for invaluable comments, which significantly improved the manuscript. The ASTE telescope is operated by National Astronomical Observatory of Japan (NAOJ). We would like to acknowledge all of the members involved with the ASTE team for their great efforts in the ASTE project. This study was financially supported by MEXT Grant-in-Aid for Young Scientists (B) No. 24740126. This work is based on observations made with the Spitzer Space Telescope, which is operated by the Jet Propulsion Laboratory, California Institute of Technology under a contract with NASA.

References

Bayet, E., Gerin, M., Phillips, T. G., & Contursi, A. 2009, MNRAS, 399, 264

Calzetti, D., et al. 2007, ApJ, 666, 870

Carignan, C. 1985, ApJS, 58, 107

Daddi, E., Elbaz, D., Walter, F., et al. 2010, ApJL, 714, L118

Dale, D. A., Cohen, S. A., Johnson, L. C., et al. 2009, ApJ, 703, 517

Dumke, M., Nieten, C., Thuma, G., Wielebinski, R., & Walsh, W. 2001, A&A, 373, 853

Emerson, D. T., & Graeve, R. 1988, A&A, 190, 353

Ezawa, H., Kawabe, R., Kohno, K., & Yamamoto, S. 2004, Proc. SPIE, 5489, 763

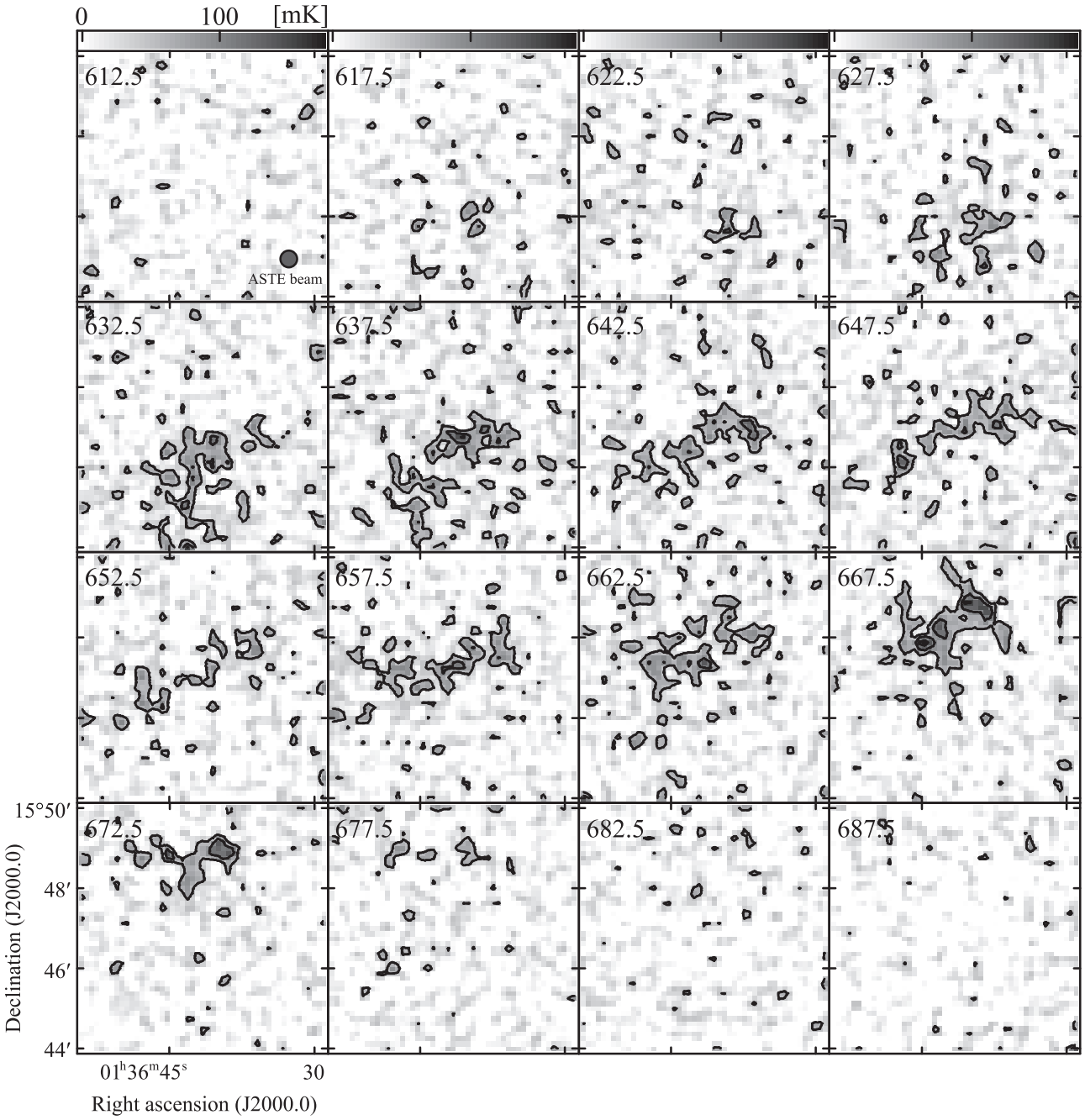


Fig. 2. Velocity channel maps of CO($J = 3 - 2$) emission in NGC 628. The contour levels are 2, 4, and 6σ, where 1σ = 25 mK in $T_{\rm MB}$ scale. The velocity width of each channel is 5 km s^{-1}, and the central velocities ($V_{\rm LSR}$ in km s^{-1}) are labeled in the top-left corner of each map. The beam size of the ASTE (25″) is indicated in the bottom-right corner of the first panel.

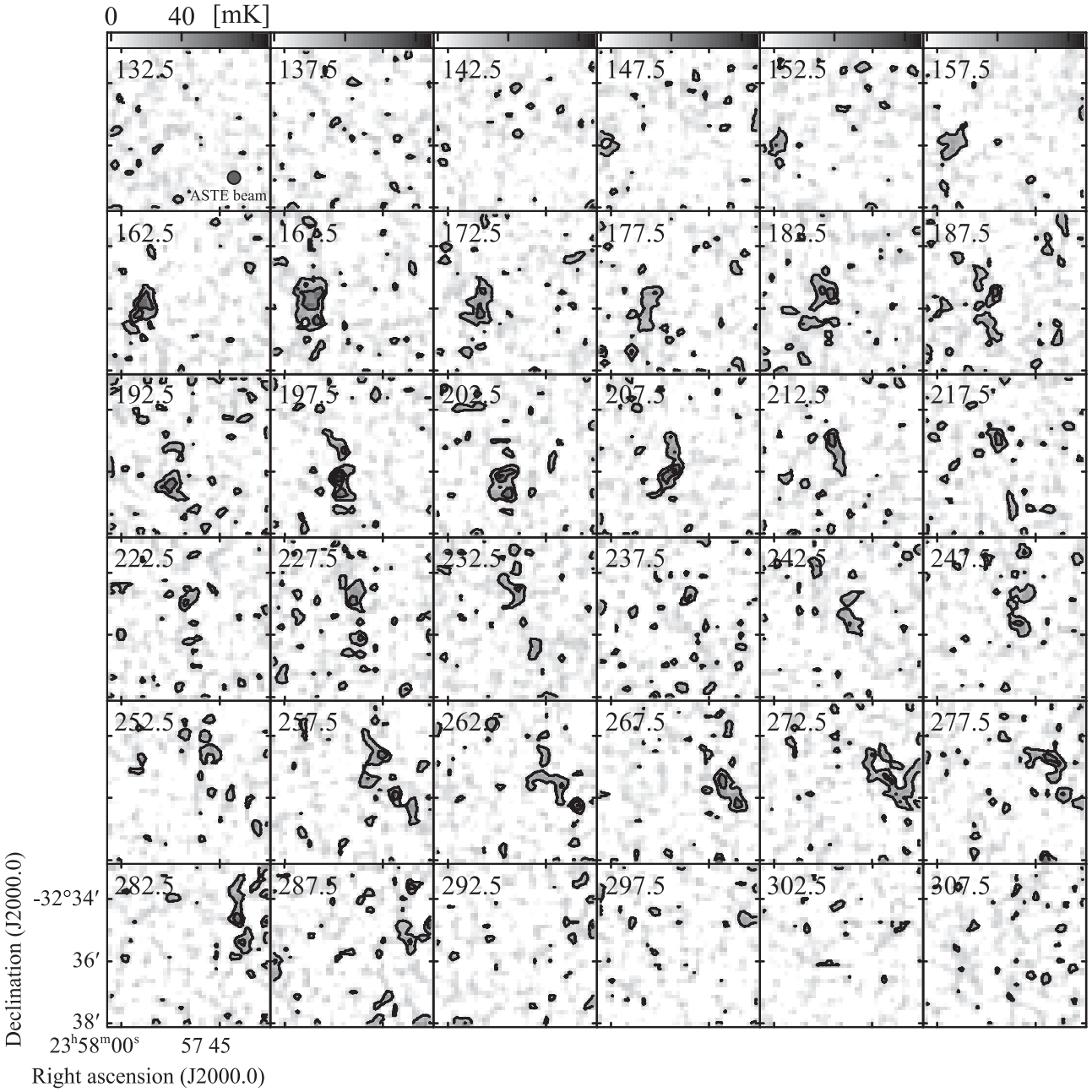


Fig. 3. Velocity channel maps of CO($J = 3 - 2$) emission in NGC 7793. The contour levels are 2, 4, 6, and 8σ, where 1σ = 11 mK in $T_{\rm MB}$ scale. The velocity width of each channel is 5 km s^{-1}, and the central velocities ($V_{\rm LSR}$ in km s^{-1}) are labeled in the top-left corner of each map. The beam size of the ASTE (25″) is indicated in the bottom-right corner of the first panel.

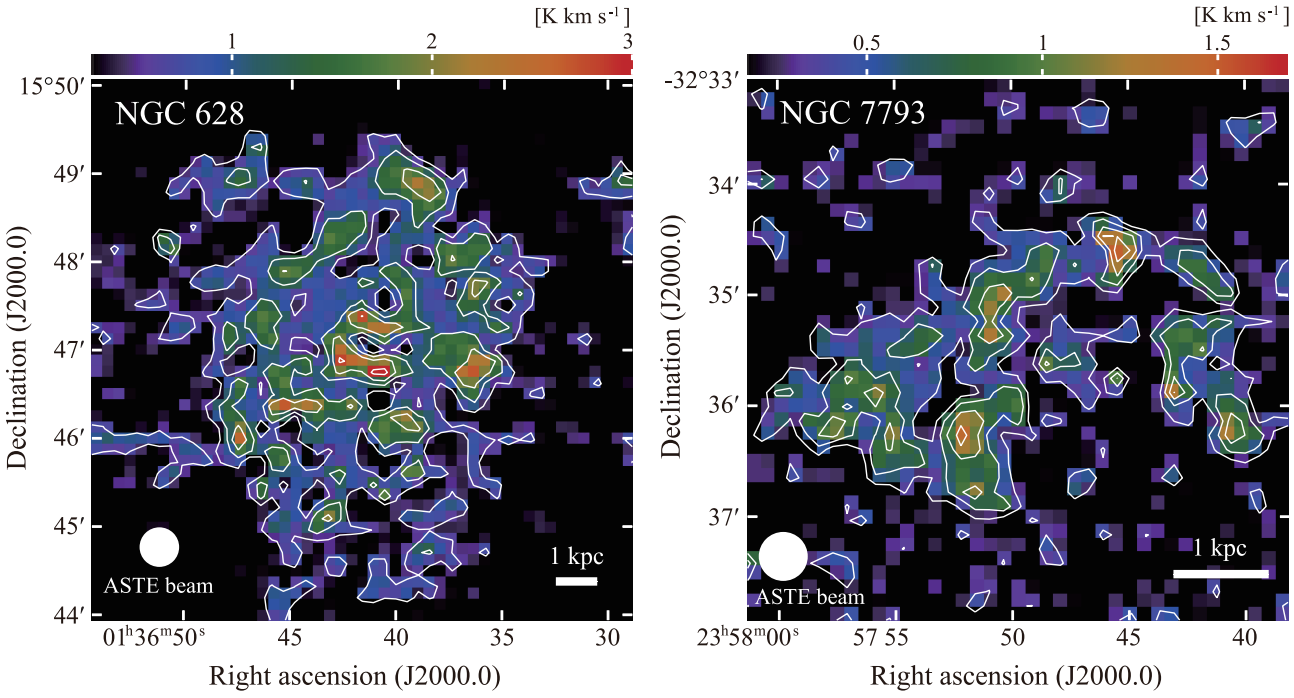


Fig. 4. Maps of velocity-integrated CO($J = 3 - 2$) intensities in NGC 628 (left) and NGC 7793 (right). The contour levels are 2, 4, 6, and 9σ, where 1σ = 0.30 K km s^{-1} in $T_{\rm MB}$ scale for NGC 628, and those are 2, 4, 6, and 8σ, where 1σ = 0.16 K km s^{-1} in $T_{\rm MB}$ scale for NGC 7793, respectively. The beam size of the ASTE (25″) is indicated in the bottom-left corner of each map.

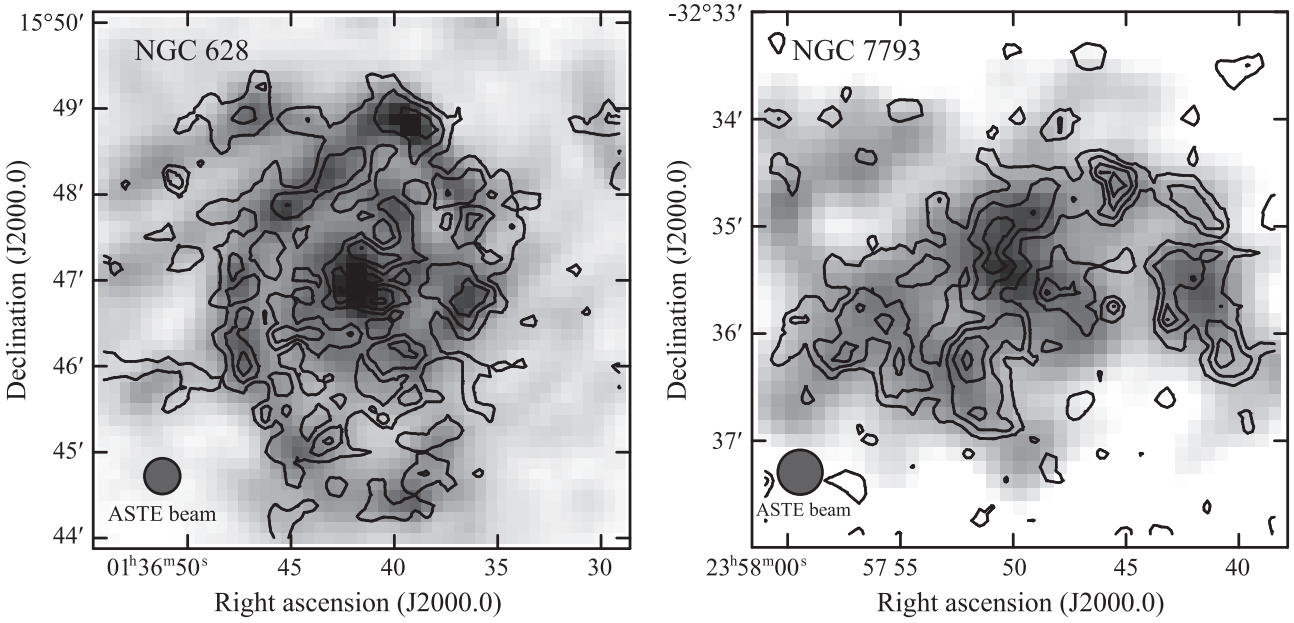


Fig. 5. Maps of velocity-integrated CO($J = 3 - 2$) intensities (contours) superposed on $Herschel$/SPIRE 350 μm images (gray scale) obtained by (Kennicutt et al. 2011) for NGC 628 (left) and NGC 7793 (right). The contour levels are the same as figure 4. The beam size of the ASTE (25″) is indicated in the bottom-left corner of each map.

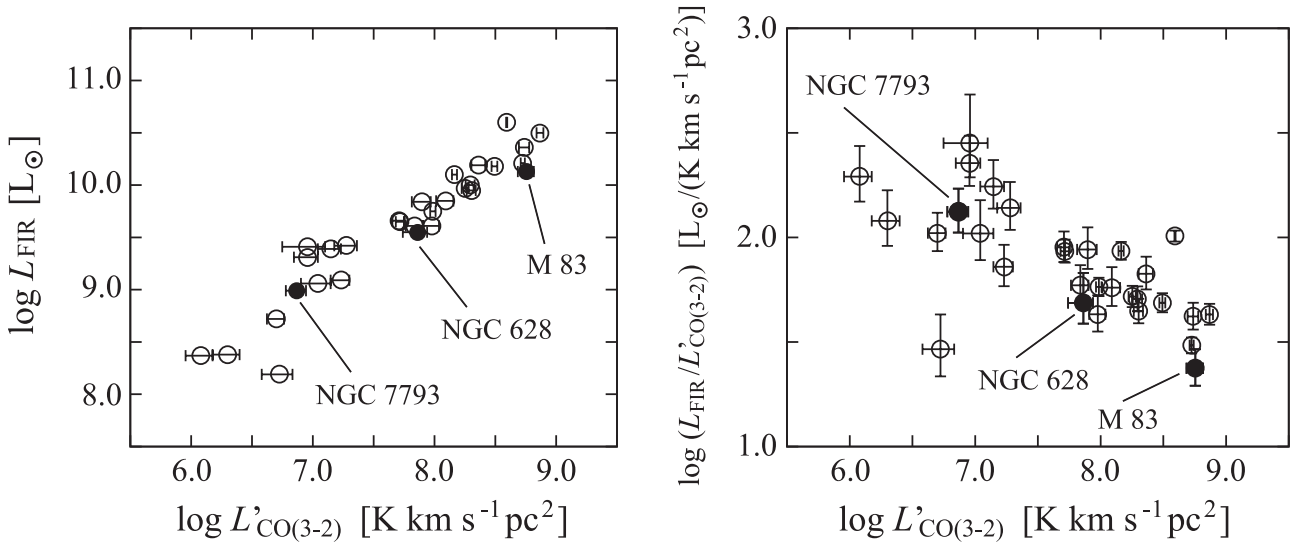


Fig. 6. A correlation between the global $L'_{\rm CO(3-2)}$ and $L_{\rm FIR}$ (left) and the variation in $L_{\rm FIR}/L'_{\rm CO(3-2)}$ as a function of $L'_{\rm CO(3-2)}$ (right) for our ASTE sample (filled circles) and the JCMT NGLS sample (Wilson et al. 2012; open circles).

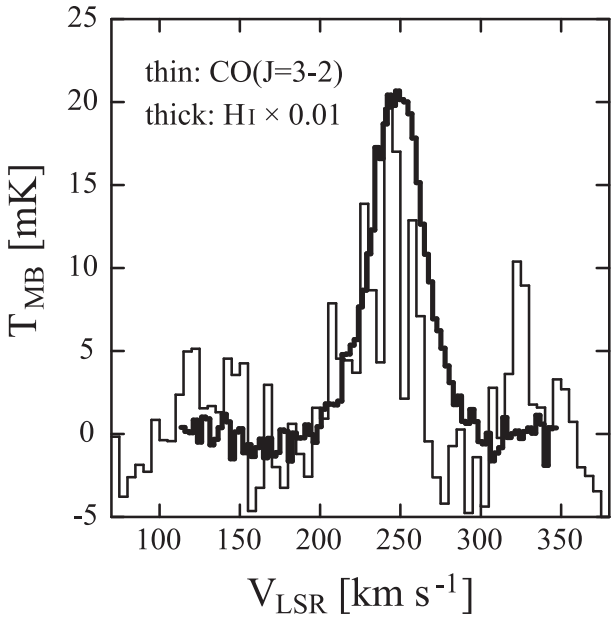


Fig. 7. Spectra of the convolved CO($J = 3 - 2$) emission (thin line) and the H I emission (Walter et al. 2008; thick line) at the angular resolution of 43″ in the central region of NGC 7793. The temperature scale of H I emission is multiplied by 0.01 for display.

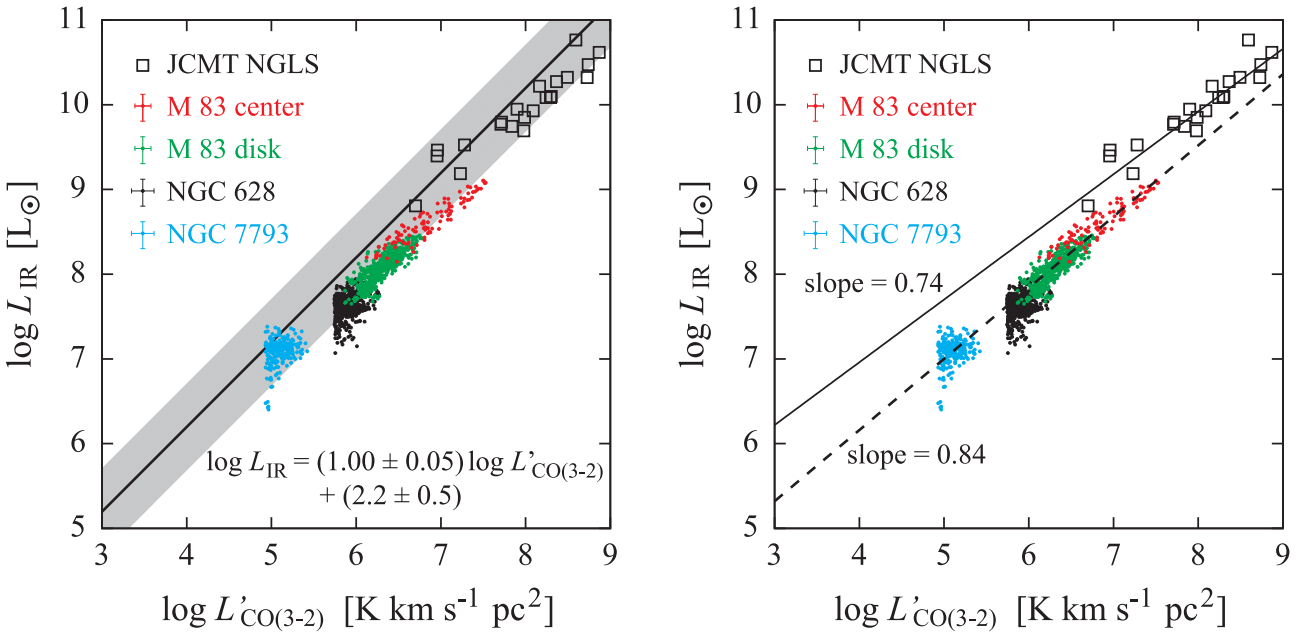


Fig. 8. (left) A correlation between $L'_{\rm CO(3-2)}$ and $L_{\rm IR}$. Typical errors due to the calibration uncertainty are shown in the next of each galaxy name. The solid line and the shaded area indicate the best-fit relation with its error for the local (U)LIRGs and submillimeter selected dusty star-forming galaxies (Greve et al. 2014). (right) Same as left panel, but the solid line indicates the best-fit slope for JCMT NGLS sample, and the dashed line indicates that for our spatially-resolved sample.

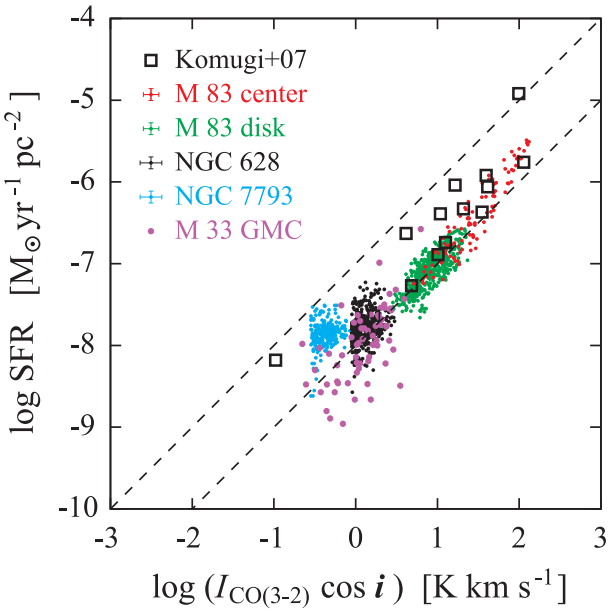


Fig. 9. A correlation between inclination-corrected $I_{\rm CO(3-2)}$ and SFRs. Typical errors due to the calibration uncertainty are shown in the next of each galaxy name. Data points of M 33 are derived from CO($J = 1 - 0$) peak positions of individual GMCs Onodera et al. (2012). Each dashed line indicates a linear correlation (not best-fit for data points) in this plot.

Table 1. Galaxy parameters

Galaxy name	NGC 628	NGC 7793
Morphological type[a]	SA(s)c	SA(s)d
Map center[b]:		
Right Ascension	$1^{\rm h}36^{\rm m}41^{\rm s}.7$	$22^{\rm h}57^{\rm m}49^{\rm s}.8$
Declination	$15^\circ47'00''.5$	$-32^\circ35'27''.7$
Distance[c]	7.3 Mpc	3.91 Mpc
Linear scale	36 pc arcsec^{-1}	19 pc arcsec^{-1}
Inclination[d]	$6^\circ.5$	$53^\circ.7$
12 + log(O/H)[e]	8.78	8.50
H_2 mass[f,g]	$1.51 \times 10^9\ M_\odot$	$2.0 \times 10^8\ M_\odot$
H I mass[f]	$7.43 \times 10^9\ M_\odot$	$1.05 \times 10^9\ M_\odot$
stellar mass[h]	$1.48 \times 10^{10}\ M_\odot$	$3.72 \times 10^9\ M_\odot$
global SFR[i]	0.59 $M_\odot$ yr^{-1}	0.30 $M_\odot$ yr^{-1}
specific SFR	3.99×10^{-11} yr^{-1}	8.06×10^{-11} yr^{-1}
$L_{\rm FIR}$ $(4-400\ \mu{\rm m})$[j]	$3.53 \times 10^9\ L_\odot$	$9.81 \times 10^8\ L_\odot$
$L_{\rm IR}$ $(8-1000\ \mu{\rm m})$[j]	$4.76 \times 10^9\ L_\odot$	$1.10 \times 10^9\ L_\odot$

[a]Morphological type from RC3. [b]Map center from Jarrett et al. (2003). [c]Adopted distances from Karachentsev et al. (2004). [d]Inclination for NGC 628 from Kamphuis & Briggs (1992) and NGC 7793 from Carignan (1985). [e]Metallicity form Garnett (2002). [f]H_2 mass for NGC 628 and H I masses for NGC 628 and NGC 7793 are calculated from the original data presented by Garnett (2002) for adopted distances. [g]H_2 mass for NGC 7793 is calculated from the central CO($J = 1-0$) intensity obtained by Israel et al. (1995) assuming the ratio of central to total H_2 mass being 0.05. [h]stellar masses are calculated from the equation (8) in Querejeta et al. (2015) using $Spitzer$/IRAC 3.6 μm and 4.5 μm fluxes presented by Dale et al. (2009). [i]global SFR from Kennicutt et al. (2008). [j]$L_{\rm FIR}$ and $L_{\rm IR}$ are calculated from the original data presented by Sanders et al. (2003) for adopted distances.

Ezawa, H., et al. 2008, Proc. SPIE, 7012,

Gao, Y., & Solomon, P. M. 2004, ApJ, 606, 271

Garnett, D. R. 2002, ApJ, 581, 1019

Goldreich, P., & Kwan, J. 1974, ApJ, 189, 441

Greve, T. R., Leonidaki, I., Xilouris, E. M., et al. 2014, ApJ, 794, 142

Helfer, T. T., Thornley, M. D., Regan, M. W., et al. 2003, ApJS, 145, 259

Hollenbach, D. J., & Tielens, A. G. G. M. 1997, ARA&A, 35, 179

Hollenbach, D. J., & Tielens, A. G. G. M. 1999, Reviews of Modern Physics, 71, 173

Inoue, H., Muraoka, K., Sakai, T., Endo, A., Kohno, K., Asayama, S., Noguchi, T., and Ogawa, H. 2008, in

Table 2. Observation parameters

Galaxy name	NGC 628	NGC 7793
Observation date	September to October, 2013	July to August, 2014
Total observation time	30 hours	50 hours
Field coverage	$6' \times 6'$ (12.8 $\times$ 12.8 kpc)	$5' \times 5'$ (5.8 $\times$ 5.8 kpc)
System noise temperature	$250 - 300$ K	$200 - 250$ K
Main-beam efficiency	$0.57 \pm 0.06 \pm 0.03$	$0.65 \pm 0.07 \pm 0.05$
Velocity resolution	5 km s^{-1}	5 km s^{-1}
r.m.s noise level in $T_{\rm MB}$ scale	25 mK	11 mK

For the main-beam efficiency, the first error indicates systematic error and the second, random error.

Proc. 19th International Symposium on Space Terahertz Technology, 281

Iono, D., Wilson, C. D., Yun, M. S., et al. 2009, ApJ, 695, 1537

Israel, F. P. 2005, A&A, 438, 855

Israel, F. P., Tacconi, L. J., & Baas, F. 1995, A&A, 295, 599

Jarrett, T. H., Chester, T., Cutri, R., Schneider, S. E., & Huchra, J. P. 2003, AJ, 125, 525

Kamphuis, J., & Briggs, F. 1992, A&A, 253, 335

Karachentsev, I. D., Karachentseva, V. E., Huchtmeier, W. K., & Makarov, D. I. 2004, AJ, 127, 2031

Kaufman, M. J., Wolfire, M. G., Hollenbach, D. J., & Luhman, M. L. 1999, ApJ, 527, 795

Kennicutt, R. C., Jr. 1998a, ApJ, 498, 541

Kennicutt, R. C., Jr. 1998b, ARA&A, 36, 189

Kennicutt, R. C., Jr., Armus, L., Bendo, G., et al. 2003, PASP, 115, 928

Kennicutt, R. C., Calzetti, D., Aniano, G., et al. 2011, PASP, 123, 1347

Kennicutt, R. C., Jr., Lee, J. C., Funes, S. J., José G., Sakai, S., & Akiyama, S. 2008, ApJS, 178, 247

Kohno, K., et al. 2008, PASJ, 60, 457

Komugi, S., Kohno, K., Tosaki, T., Nakanishi, H., Onodera, S., Egusa, F., & Sofue, Y. 2007, PASJ, 59, 55

Krumholz, M. R., Dekel, A., & McKee, C. F. 2012, ApJ, 745, 69

Leroy, A. K., Walter, F., Sandstrom, K., et al. 2013, AJ, 146, 19

Liu, D., Gao, Y., Isaak, K., et al. 2015, ApJL, 810, L14

Mao, R.-Q., Schulz, A., Henkel, C., et al. 2010, ApJ, 724, 1336

Mauersberger, R., Henkel, C., Walsh, W., & Schulz, A. 1999, A&A, 341, 256

Meier, D. S., Turner, J. L., Crosthwaite, L. P., & Beck, S. C. 2001, AJ, 121, 740

Miura, R. E., Kohno, K., Tosaki, T., et al. 2012, ApJ, 761, 37

Miura, R. E., Kohno, K., Tosaki, T., et al. 2014, ApJ, 788, 167

Muraoka, K., Kohno, K., Tosaki, T., et al. 2009, ApJ, 706, 1213

Muraoka, K., et al. 2007, PASJ, 59, 43

Narayanan, D., Groppi, C. E., Kulesa, C. A., & Walker, C. K. 2005, ApJ, 630, 269

Oka, T., Nagai, M., Kamegai, K., Tanaka, K., & Kuboi, N. 2007, PASJ, 59, 15

Onodera, S., Kuno, N., Tosaki, T., et al. 2012, PASJ, 64, 133

Querejeta, M., Meidt, S. E., Schinnerer, E., et al. 2015, ApJS, 219, 5

Sanders, D. B., Mazzarella, J. M., Kim, D.-C., Surace, J. A., & Soifer, B. T. 2003, AJ, 126, 1607

Sanders, D. B., Scoville, N. Z., Tilanus, R. P. J., Wang, Z., & Zhou, S. 1993, Back to the Galaxy, 278, 311

Sawada, T., et al. 2008, PASJ, 60, 445

Schmidt, M. 1959, ApJ, 129, 243

Scoville, N. Z. & Solomon, P. M. 1974, ApJ, 187, L67

Sorai, K., Sunada, K., Okumura, S. K., Tetsuro, I., Tanaka, A., Natori, K., & Onuki, H. 2000b, Proc. SPIE, 4015, 86

Thim, F., Tammann, G. A., Saha, A., Dolphin, A., Sandage, A., Tolstoy, E., & Labhardt, L. 2003, ApJ, 590, 256

Tosaki, T., Miura, R., Sawada, T., Kuno, N., Nakanishi, K., Kohno, K., Okumura, S. K., & Kawabe, R. 2007b, ApJL, 664, L27

Vlahakis, C., van der Werf, P., Israel, F. P., & Tilanus, R. P. J. 2013, MNRAS, 433, 1837

Walter, F., Brinks, E., de Blok, W. J. G., et al. 2008, AJ, 136, 2563

Wang, Y., Jaffe, D. T., Graf, U. U., & Evans, N. J., II 1994, ApJS, 95, 503

Warren, B. E., Wilson, C. D., Israel, F. P., et al. 2010, ApJ, 714, 571

Wilson, C. D., Warren, B. E., Israel, F. P., et al. 2009, ApJ, 693, 1736

Wilson, C. D., Warren, B. E., Israel, F. P., et al. 2012, MNRAS, 424, 3050

Yao, L., Seaquist, E. R., Kuno, N., & Dunne, L. 2003, ApJ, 588, 771